Journal of Virology

A Viral Protein Mediates Superinfection Exclusion at the Whole-Organism Level but Is Not Required for Exclusion at the Cellular Level

María Bergua, Mark P. Zwart, Choaa El-Mohtar, Turksen Shilts, Santiago F. Elena and Svetlana Y. Folimonova

J. Virol. **2014, 88(19):11327. DOI: 10.1128/JVI.01612-14. Published Ahead of Print 16 July 2014.**

JVI Journals.ASM.org

A Viral Protein Mediates Superinfection Exclusion at the Whole-Organism Level but Is Not Required for Exclusion at the Cellular Level

María Bergua,[a] Mark P. Zwart,[b] Choaa El-Mohtar,[c] Turksen Shilts,[c] Santiago F. Elena,[b,d] Svetlana Y. Folimonova[a]

University of Florida, Department of Plant Pathology, Gainesville, Florida, USA[a]; Instituto de Biología Molecular y Celular de Plantas (CSIC-UPV), València, Spain[b]; University of Florida, Citrus Research and Education Center, Lake Alfred, Florida, USA[c]; The Santa Fe Institute, Santa Fe, New Mexico, USA[d]

ABSTRACT

Superinfection exclusion (SIE), the ability of an established virus infection to interfere with a secondary infection by the same or a closely related virus, has been described for different viruses, including important pathogens of humans, animals, and plants. Citrus tristeza virus (CTV), a positive-sense RNA virus, represents a valuable model system for studying SIE due to the existence of several phylogenetically distinct strains. Furthermore, CTV allows SIE to be examined at the whole-organism level. Previously, we demonstrated that SIE by CTV is a virus-controlled function that requires the viral protein p33. In this study, we show that p33 mediates SIE at the whole-organism level, while it is not required for exclusion at the cellular level. Primary infection of a host with a fluorescent protein-tagged CTV variant lacking p33 did not interfere with the establishment of a secondary infection by the same virus labeled with a different fluorescent protein. However, cellular coinfection by both viruses was rare. The obtained observations, along with estimates of the cellular multiplicity of infection (MOI) and MOI model selection, suggested that low levels of cellular coinfection appear to be best explained by exclusion at the cellular level. Based on these results, we propose that SIE by CTV is operated at two levels—the cellular and the whole-organism levels—by two distinct mechanisms that could function independently. This novel aspect of viral SIE highlights the intriguing complexity of this phenomenon, further understanding of which may open up new avenues to manage virus diseases.

IMPORTANCE

Many viruses exhibit superinfection exclusion (SIE), the ability of an established virus infection to interfere with a secondary infection by related viruses. SIE plays an important role in the pathogenesis and evolution of virus populations. The observations described here suggest that SIE could be controlled independently at different levels of the host: the whole-organism level or the level of individual cells. The p33 protein of citrus tristeza virus (CTV), an RNA virus, was shown to mediate SIE at the whole-organism level, while it appeared not to be required for exclusion at the cellular level. SIE by CTV is, therefore, highly complex and appears to use mechanisms different from those proposed for other viruses. A better understanding of this phenomenon may lead to the development of new strategies for controlling viral diseases in human populations and agroecosystems.

Superinfection exclusion (SIE), a phenomenon in which a primary virus infection prevents a secondary infection by the same or a closely related virus, has been reported in a broad range of bacterial, plant, and animal viruses (1–10). Among them are important pathogens of humans, such as human immunodeficiency virus (HIV) (11), hepatitis C virus (HCV) (12), West Nile virus (13), and rubella virus (14). From the standpoint of virus evolution, SIE has been suggested to be a mechanism to reduce competition for resources (15, 16) and to maintain the stability of viral sequences due to the prevention of recombination events between related strains coinfecting the same cell (17, 18). The latter property of the exclusion phenomenon itself has clear implications for treating viral infections. If viruses could successfully superinfect cells, recombination would greatly increase virus variability. This increased variability could, in turn, result in the enhanced evolution of drug and vaccine resistance, thus compromising the development of antivirus treatments. The significance of SIE for mitigation of the effects of virus infection has also been shown for plant viruses. In what is referred to as cross-protection, crops are purposefully infected with a mild isolate as a protective measure against other virus variants that cause severe disease (7, 10). This widely accepted practice in agriculture has been an effective antiviral management procedure that has allowed the economical production of various crops.

In spite of the importance of SIE in viral pathogenesis, our understanding of how virus variants exclude each other is largely incomplete. With animal and human viruses, studies of SIE mechanisms were carried out mostly in cell cultures, thus avoiding the possibility of the exclusion effect being masked by an interferon response as well as other complications related to the nature of these pathosystems (9, 12, 14, 19). The research demonstrated that exclusion could result from impairments of different steps of the viral life cycle during superinfection, including downregulation of

Received 4 June 2014 Accepted 14 July 2014
Published ahead of print 16 July 2014
Editor: A. Simon
Address correspondence to Svetlana Y. Folimonova, svetlana@ufl.edu.

doi:10.1128/JVI.01612-14

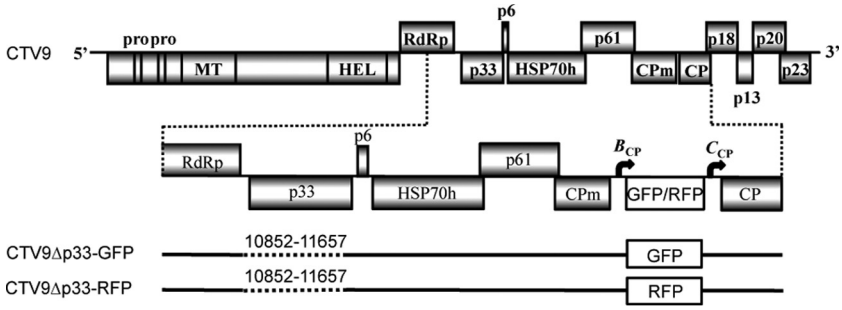

FIG 1 Schematic diagram of the genome of wild-type CTV (CTV9), CTV9Δp33-GFP, and CTV9Δp33-RFP. Open boxes, ORFs and their translation products; pro, papain-like protease domain; MT, methyltransferase; HEL, helicase; RdRp, an RNA-dependent RNA polymerase; HSP70h, HSP70 homolog; CPm, minor coat protein; CP, major coat protein; GFP, green fluorescent protein; RFP, red fluorescent protein; bent arrows, positions of beet yellows virus CP (B_{CP}) or CTV CP (C_{CP}) sgRNA controller elements. An enlarged view of the region containing the p33 ORF and schematic diagrams of the CTV mutants are shown below. The sequences deleted in the mutants are indicated by dotted lines with the corresponding nucleotide numbers.

cell surface viral receptors after primary virus infection, which affects secondary virus attachment, or interference with incoming virus penetration into the cell or with incoming virus replication and/or translation (1–3, 5, 9, 12, 19). Such mechanisms apparently function at the level of cells that were preinfected with the primary virus, and, thus, it is not clear how, if at all, they relate to SIE at the organism level. Interestingly, while many animal viruses show SIE at the cellular level, the ability to exclude secondary infection by the same or a closely related virus at the whole-organism level varies for different viruses. For instance, it was shown that HIV exhibits SIE only at the cellular level, while it permits superinfection by different virus strains at the level of an organism (reviewed in reference 20). On the other hand, with Borna disease virus as well as HCV and hepatitis B virus, SIE has been observed at the cellular level and in intact host organisms as well: in experimentally infected animals or in highly susceptible individuals (8, 12, 17, 19, 21–23). Collectively, these observations suggest that when it is occurring at both levels, the exclusion could be controlled by different mechanisms.

Plant viruses have provided more opportunities to examine the SIE phenomenon at the whole-organism level (7, 10). Most cases of homologous interference have been attributed to the induction of RNA silencing by the primary virus, an antiviral host defense mechanism that degrades the challenge virus RNA in a sequence-specific manner (7, 24, 25). RNA silencing can function systemically in cells containing the primary virus as well as in uninfected cells and, therefore, could explain SIE at both the cellular and the organism levels, in contrast to the mechanisms proposed for animal viruses (7, 24–27). However, mechanisms of SIE associated with both plant and animal viruses have not been elucidated.

We are examining SIE by citrus tristeza virus (CTV), a member of the genus *Closterovirus*, family *Closteroviridae*, which contains the largest and most complex positive-strand RNA viruses of higher plants (28–32). CTV has long flexuous virions (2,000 nm by 10 to 12 nm) encapsidated by two coat proteins and a single-stranded RNA genome of approximately 19.3 kb that encodes 12 open reading frames (ORFs) (33, 34) (Fig. 1). ORFs 1a and 1b are expressed from the genomic RNA and encode polyproteins involved in virus replication. Ten 3′-end ORFs are expressed by 3′ coterminal subgenomic RNAs (sgRNAs) (35, 36) and encode the following proteins: major coat protein (CP), minor coat protein (CPm), p65 (HSP70 homolog), and p61, which are involved in assembly of virions (37); a hydrophobic p6 protein with a proposed role in virus movement (32, 38); p20 and p23, which along with CP are suppressors of RNA silencing (39); and p33, p13, and p18, which function in extending the virus host range (40). Trees of most citrus varieties can be infected by mutants with three genes deleted: p33, p18, and p13 (38).

CTV represents a valuable model system for studying SIE due to the existence of numerous well-characterized isolates belonging to several phylogenetically distinct strains (41). Furthermore, CTV allows the study of SIE at the whole-organism level, in contrast to most animal virus systems. Additionally, CTV-based constructs show remarkable stability. The virus is able to maintain and continually express inserted reporter genes in a host for many generations over extended periods of time, which thus far have been shown to be longer than 9 years (42, 43). This feature of CTV constructs makes them excellent tools for the examination of SIE, leaving interpretation of results free from confusion due to a potential loss of a reporter-encoding insert (44, 45).

Recently, we demonstrated that SIE by CTV occurs only between isolates of the same strain and not between isolates of different strains of the virus (44). It is a powerful mechanism that completely prevents superinfection by a homologous virus from the same virus strain. Moreover, the exclusion phenomenon appears to be systemic and functions not only in cells infected with the primary virus but also in cells that were not infected. Further data demonstrated that SIE by CTV requires production of a specific viral protein, p33 (45). The lack of a functional p33 completely eliminates the ability of the virus to exclude superinfection by the same or closely related viruses. The p33 protein appears to function in a homology-dependent manner, such that its substitution with a cognate protein from a heterologous strain does not confer exclusion, suggesting the existence of precise interactions of the p33 protein with other factors involved in this phenomenon (45).

In this work, we show that the p33 protein mediates SIE at the whole-organism level, while it does not appear to be required for exclusion at the cellular level. Using two CTV variants that were tagged with green or red fluorescent protein (GFP or RFP, respectively) and that were both lacking the p33 protein, we demonstrated that although primary infection of a host with one CTV variant did not interfere with the establishment of a secondary infection with the other virus at the whole-organism level, the vast majority of the infected cells contained only one virus variant. Calculations of the cellular multiplicity of infection (MOI) to-

gether with MOI model selection and an analysis of the spatial distribution of cells infected by the two virus variants lacking the p33 protein suggested that exclusion at the cellular level was still in place.

MATERIALS AND METHODS

Virus isolates and inoculation of citrus trees. The GFP-tagged p33 deletion mutant CTV9Δp33-GFP (38, 45) and the RFP-tagged p33 deletion mutant CTV9Δp33-RFP, described below, have been maintained in citrus plants under greenhouse conditions. These plants were used as sources of virus for subsequent graft inoculations of young trees to assess SIE as described previously (44, 45).

Generation of CTV9Δp33-RFP. The full-length cDNA clone of CTV T36 pCAM:CTV947R (46) and the GFP-tagged cDNA clone CTV-BC5/GFP (42) were the basis for engineering the RFP-tagged p33 deletion mutant construct. The RFP (TagRFP) reporter gene mobilized in the pSITEII-C1 vector (47), kindly provided by M. M. Goodin (University of Kentucky, Lexington, KY), was amplified using primers designed to incorporate PacI and XhoI restriction endonuclease sites at the 5′ and 3′ ends, respectively. The PCR-amplified RFP ORF digested with PacI and XhoI was introduced into the CTV-BC5/GFP vector digested with the same enzymes. The resulting CTV-BC5/RFP construct was digested with PmeI and PstI endonucleases (nucleotide positions 11869 to 11876 and 17208 to 17213 in the genome of T36, respectively). The fragment containing the RFP ORF was substituted for the corresponding fragment in pCAMΔp33 9-47R modified from the original binary vector construct, pCAM:CTV947R (46), to create a deletion within the p33 gene, as described by Tatineni et al. (38), and to introduce the ORF of the p22 silencing suppressor of tomato chlorosis virus (48) by replacing the hygromycin gene in the pCAMBIA 1380 backbone at the XhoI site. The new construct was named pCTV9Δp33-RFP.

In order to accumulate CTV9Δp33-RFP virions for inoculation of citrus plants, the respective construct was first transfected into *Agrobacterium tumefaciens* cells. The bacterial cultures carrying pCTV9Δp33-RFP binary plasmids were used for infiltration of *Nicotiana benthamiana* plants as described earlier (46, 49). One week after infiltration, CTV9Δp33-RFP virions were extracted from the infiltrated leaves, concentrated by centrifugation on a sucrose cushion, and used for inoculation of the bark flap of *Citrus macrophylla* seedlings according to the procedure described earlier (50).

Serological assays. Double-antibody sandwich enzyme-linked immunosorbent assay (ELISA) of tissue extracts was performed as described previously using antibodies specific to CTV virions (44, 45, 51) to confirm infection in inoculated plants.

Examination of fluorescence in citrus plants infected with RFP- or GFP-tagged viruses. Bark tissues from trees inoculated with CTV9Δp33-RFP and/or CTV9Δp33-GFP were examined for RFP and GFP fluorescence at different times beginning at 4 weeks after primary infection and at 6 weeks after challenge using a Zeiss Stemi SV 11 UV fluorescence dissecting microscope (Carl Zeiss Jena).

Confocal laser scanning microscopy. Samples of bark tissue from different flushes of five individual *C. macrophylla* trees infected with CTV9Δp33-RFP and/or CTV9Δp33-GFP were collected at the time point corresponding to 12 weeks after challenge inoculation with the secondary virus. This time is enough for the second virus to get established in a tree under the conditions in which no SIE at the host level occurs. Importantly, samples were taken from the newly developed systemic tissues, which can be colonized by both viruses. The samples were observed using a confocal laser scanning fluorescence microscope (TCS SL; Leica, Heidelberg, Germany). GFP and RFP were excited by using 488- and 543-nm laser lines, respectively. When using multiple fluorophores simultaneously, images were acquired sequentially, line by line, in order to reduce excitation and emission cross talk. Exposure settings that minimized oversaturated pixels in the final images were used. A Leica HC PL Fluotar ×10.0/0.30 objective was used. Image acquisition was conducted at a resolution of 512 by 512 pixels. A total of 10 z-stacks comprising 50 optical sections were taken using samples of bark tissue for each treatment (z-step width, 2.5 μm). The number of cells infected by CTV9Δp33-RFP and/or CTV9Δp33-GFP in each z-stack was determined by visual inspection of CTV9Δp33-RFP or CTV9Δp33-GFP in the red or green channel, respectively, using ImageJ software (http://rsb.info.nih.gov/ij/). Five sequential optical sections at different depths within the z-stack (sections 8 to 12, 18 to 22, 28 to 32, and 38 to 42) were merged separately in the green and red channels to count the number of cells infected by each virus instead of using a whole z-stack projection of 50 sections. The total number of cells was obtained by adding the number of cells found in each set of the merged sections. Caution was taken in order to avoid counting the same cell twice on the merged sections at different depths within the z-stack. Images obtained in the green and red channels were superimposed to reveal cells doubly infected with RFP- and GFP-tagged viruses (yellow cells). A cell was counted as coinfected with the two virus variants if the distribution and intensity of GFP and RFP fluorescence throughout the cell observed in the green and red channels, respectively, were comparable. Cell coinfection was confirmed by colocalization analysis using Colocalization ImageJ plug-in software.

MOI calculation. The MOI was calculated by fitting the observed count data to the so-called model 1 described previously (52) and originally proposed elsewhere (53). This model assumes that the number of infecting virions, considered only over the virus-infected cells, takes a constant value of m_I and that the proportion of cells infected only by the CTV9Δp33-RFP variant is then given by the zero term of a binomial distribution of the number of infecting virions of the CTV9Δp33-GFP variant:

$$\Pr(\mathrm{GFP} = g) = \binom{m_I}{g} p_{\mathrm{GFP}}^{g} (1 - p_{\mathrm{GFP}})^{m_I - g}$$

where Pr is the expected probability, g is an observation of CTV9Δp33-GFP-infected cells, and p_{GFP} is the frequency of the CTV9Δp33-GFP-infected cells, estimated from the data as

$$p_{\mathrm{GFP}} = 1 - p_{\mathrm{RFP}} = \left[f\left(\mathrm{GFP} \cap \overline{\mathrm{RFP}}\right) + f\left(\mathrm{GFP} \cap \mathrm{RFP}\right) \right] / \left[f\left(\mathrm{GFP} \cap \overline{\mathrm{RFP}}\right) + f\left(\overline{\mathrm{GFP}} \cap \mathrm{RFP}\right) + 2f\left(\mathrm{GFP} \cap \mathrm{RFP}\right) \right]$$

where p_{RFP} is the frequency of the CTV9Δp33-RFP-infected cells, and $f(\cdot)$ denotes the observed frequencies of each class of infected cells. Given that m_I is constant, the expected frequency of cells coinfected by both variants in the fraction of infected cells is just given by $1 - p_{GFP}^{m_I} - p_{RFP}^{m_I}$. The predicted frequency of singly and mixed-variant infected cells can then be compared to the observed frequency by means of a G likelihood ratio test (54).

MOI model selection. Model selection was first performed for a set of four models described previously (52) and afterwards for a set of two models (models 2 and 4). Model 2 is the null model and assumes that the distribution of infecting viruses follows a Poisson distribution, such that $\Pr(K = k) = m_T^k e^{-m_T}/k!$, where m_T is the number of infecting virions over all cells, K is a random variable denoting the number of viruses infecting a cell, and k is a realization of this random variable (i.e., a particular value taken by K). It then follows that the expected frequency of cellular coinfections in infected cells is (52)

$$f\left(\mathrm{GFP} \cap \mathrm{RFP}\right) = \left(1 - e^{-m_T p_{\mathrm{GFP}}}\right)\left(1 - e^{-m_T (1 - p_{\mathrm{GFP}})}\right)$$

To predict $f(\mathrm{GFP} \cap \mathrm{RFP})$ from the data, we use the relationship between m_T and the predicted fraction of uninfected cells:

$$m_T = -\ln\left[f\left(\overline{\mathrm{GFP}} \cap \overline{\mathrm{RFP}}\right) \right]$$

We could not quantify the total number of susceptible cells, and, moreover, not all phloem-associated cells appear to be susceptible to infection (55). We therefore took the highest number of infected cells observed for one sample (176 cells for CTV9Δp33-GFP; see Table 1) to be the maximum number of susceptible cells, κ. This number is an outlier, and the actual number for each sample is therefore likely to be lower, but this

makes our analysis conservative with respect to whether SIE occurs (i.e., if the actual number of susceptible cells is slightly lower, we would expect more cellular coinfection and the discrepancy between model 2 and the data would become larger, more strongly favoring alternative models). Therefore, $f(\text{GFP} \cap \text{RFP})$ is approximately equal to $(g + r)/\kappa$, where g and r are the numbers of CTV9Δp33-GFP- and CTV9Δp33-RFP-infected cells observed, respectively.

Model 3 assumes that the two virus variants become separated over time as the virus expands throughout the host plant (52). This segregation of virus variants will not affect m_T, but it will affect the frequency of cellular coinfection, such that

$$f(\text{GFP} \cap \text{RFP}) = e^{-\psi t}\left(1 - e^{-m_T p_{\text{GFP}}}\right)\left[1 - e^{-m_T(1-p_{\text{GFP}})}\right]$$

where ψ is a constant that determines that rate at which tissues are infected by only one genotype over time. Model 4 assumes that there is SIE. Since we are considering data from a single time point here, we simplify the model described previously (52) (referred to as model 5 in the previous study), such that SIE has a constant magnitude and therefore

$$m_T = -\omega \cdot \ln\left[f\left(\overline{\text{GFP}} \cap \overline{\text{RFP}}\right)\right]$$

where ω is a constant that determines the strength of SIE by lowering m_T. Model 5 combines models 3 and 4.

We performed grid searches over progressively smaller large parameter spaces to ensure global and accurate estimates of parameters. We calculated the binomial likelihood for model predictions for each sample (L) as

$$L\left(f(\text{GFP} \cap \text{RFP})|x, y\right) = \binom{x}{y} f(\text{GFP} \cap \text{RFP})^y \left[1 - f(\text{GFP} \cap \text{RFP})\right]^{x-y}$$

where x is the total number of infected cells, and y is the number of coinfected cells. The sum of the negative log likelihood (NLL) values was then used for model selection by means of the Akaike information criterion (AIC).

Spatial segregation analysis. To test if there was spatial segregation of the two virus variants at the cellular level, we considered whether the spatial distribution of the two variants over infected cells appears to be random. We first determined the Cartesian coordinates of the main areas of infection in each merged section separately for each virus variant using ImageJ (56), (i) generating an 8-bit monochrome image, (ii) reducing the image to 50 by 5 pixels (width by height; each pixel then has the approximate dimensions of one infected cell), (iii) setting the threshold values such that the background is lost (threshold value, 15), and (iv) using the ImageJ tool to determine coordinates. A .csv file of coordinates was then imported into R, version 3.0.2 (57). The arrays containing the coordinate data for the two virus variants were combined, and any repetition of pairs of coordinates was removed. The data were then resampled 1,000 times: we randomly selected N coordinates of infected cells for each virus variant, where N is the number of infected points. We then determined the distance to the nearest neighbor for each infected point (d), using the nndist procedure in the Spatstat library (58), and used these measurements to calculate R, the nearest-neighbor ratio (59):

$$R = \frac{\sum d/N}{1/2\sqrt{N/A}}$$

where A is the total area analyzed (the area of one merged section in a reduced resolution was equal to 250 pixels). The numerator is the mean distance to the nearest neighbor, whereas the denominator is the expected mean distance to the nearest neighbor for a given density. A value of R of >1 indicates overdispersion, whereas a value of R of <1 indicates aggregation. However, here we were not interested in the absolute values of R, which also depend on the spatial distribution of all infected cells, but, rather, were interested in the comparison of R values for observed and resampled data. We therefore considered whether values of R calculated for the observed data fell within the 95% confidence interval (CI) established using the resampled data. However, our analysis is based on four merged sections per virus variant per flush. To take into account the effects of multiple comparisons, we first considered which sections had observed values outside the predicted 95% CI. We then resampled the data for these sections 10,000 times, determined Holm-Bonferroni-corrected CIs (i.e., 98.75%, 98.33%, 97.5%, and 95% CIs), and then sequentially checked whether the observed R values fell within these limits, starting with the most divergent sample. The Holm-Bonferroni correction was used to account for the fact that multiple sections are tested per flush in a balanced manner.

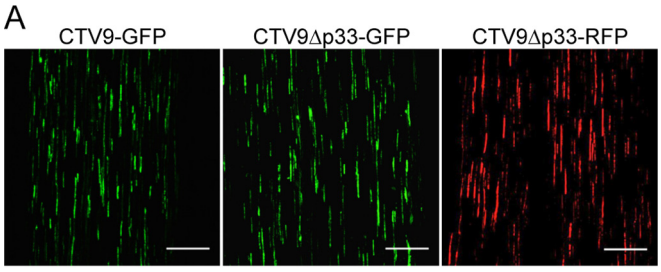

B

CTV variant	CTV titer
CTV9-GFP	2.82 ± 0.041
CTV9Δp33-GFP	2.89 ± 0.035
CTV9Δp33-RFP	2.93 ± 0.026
None	0.10 ± 0.004

FIG 2 Examination of virus infection in *C. macrophylla* trees inoculated with CTV9-GFP, CTV9Δp33GFP, or CTV9Δp33RFP. (A) Observation of GFP or RFP fluorescence in phloem-associated cells of the inoculated trees. Observations were done on the internal surface of bark at 2 months after inoculation using a confocal laser scanning fluorescence microscope. Bars = 300 μm. (B) Analysis of viral titer by double-antibody sandwich ELISA. Trees were assayed 6 weeks after initial inoculation. CTV titers (A_{405} values obtained by ELISA) are the averages of the results for 5 plants ± 1 SD.

RESULTS

Generation of CTV deletion mutants tagged with fluorescent proteins to study the distribution of virus populations in citrus trees. In our recent study, we demonstrated that modifications of the p33 gene, which restricted production of the functional protein, prevented SIE (45). In contrast to the wild-type virus, mutants with a deletion or a frameshift mutation within the p33 ORF lost the ability to exclude superinfection by the same mutants or by the wild-type virus. The primary infection with these mutants had no interference with a secondary infection, as was observed when a GFP-tagged virus was used as a challenge virus. The expression of GFP fluorescence in trees preinfected with the p33 mutants and then challenged with the GFP-marked virus was comparable to that found upon inoculation of trees with no primary infection.

Thus, the lack of production of the p33 protein resulted in the inability of the virus to exclude superinfection at the whole-plant level. Our next goal was to assess whether this observation at the plant level has a parallel at the cellular level. To examine the distribution of both the primary and challenge viruses in plant tissues upon their sequential inoculation and to be able to discriminate between them, we generated another CTV mutant, CTV9Δp33-RFP, in addition to the CTV9Δp33-GFP construct that was used in our previous experiments (45). Similar to the latter virus, CTV9Δp33-RFP contained a deletion within the p33 gene and had the ORF for a fluorescent protein, in this case, RFP, inserted be-

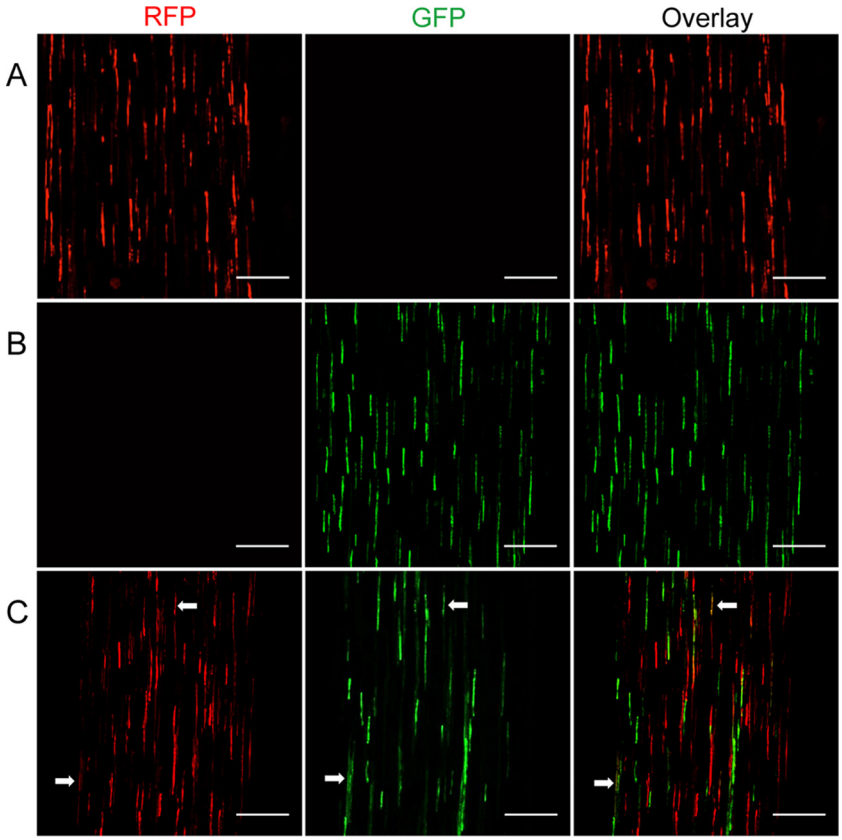

FIG 3 Observation of fluorescence in phloem-associated cells of *C. macrophylla* trees infected with CTV variants. (A) Trees were inoculated with CTV9Δp33-RFP. (B) Trees were inoculated with CTV9Δp33-GFP. (C) Trees were first inoculated with CTV9Δp33-RFP and then challenged with CTV9Δp33-GFP. Arrows, cells that are coinfected with the two virus mutants. Observations were done at 12 weeks after challenge inoculation on the internal surface of bark of the newly developed flushes using a confocal laser scanning fluorescence microscope. Bars = 300 μm.

tween the CPm and CP genes under the control of the beet yellows virus CP sgRNA promoter (Fig. 1). Both viruses had nearly identical biological properties. The infection levels of the GFP- and RFP-tagged deletion mutants, their movement and distribution, as well as their stability within host plants were similar and were also comparable to those of the wild-type virus. The CTV9Δp33-RFP and CTV9Δp33-GFP mutants established productive infection in citrus plants at similar times, which was usually about 4 to 5 weeks postinoculation, and at similar levels, as was demonstrated by the observation of GFP and RFP fluorescence in phloem tissue of the infected plants and by serological assays of the plant material (ELISA) using CTV-specific antiserum (Fig. 2). The characteristics of CTV9Δp33-RFP and CTV9Δp33-GFP were comparable to those of the GFP-tagged wild-type CTV. All three viruses reached similar titers and had a similar distribution in citrus trees, as was shown by a similar distribution of infected cells (Fig. 2). These observations were in agreement with the earlier reports, which demonstrated that CTV mutants with a deletion within the p33 ORF retain the ability to infect, multiply, and spread throughout trees of most citrus varieties at the levels of the wild-type virus (38, 45). Importantly, the viruses continuously expressed bright red or green fluorescence in infected phloem cells, allowing their visualization over extended periods of many months. These results were consistent with our previous observations of the remarkable stability of recombinant CTV vector constructs, which have demonstrated the ability to maintain and express a foreign insert in a host for more than 9 years thus far (42, 43).

Sequential inoculation of a host with viruses that lack p33 protein results in superinfection at the whole-organism level but not at the cellular level. As we demonstrated previously (45), primary infection with a CTV variant that lacks the p33 protein does not exclude superinfection by the same virus at the plant level. To assess whether the absence of p33 leads to superinfection at the cellular level, we examined the distribution of virus-infected cells upon sequential inoculation of the host trees, with the main interest being to see whether both viruses occupy the same cells or whether they are mainly confined to separate cells. Young *C. macrophylla* trees were first inoculated with the CTV9Δp33-RFP isolate by grafting virus-infected tissue into the stems of receptor trees. At 6 weeks postinoculation, systemic infection of the new leaves was confirmed by observation of RFP fluorescence and by ELISA (data not shown). The plants were challenged by placement of a second graft of tissue infected with CTV9Δp33-GFP. As a control for this experiment, another set of plants was first inoculated with CTV9Δp33-RFP but was not subjected to a secondary inoculation. An additional set of control plants with no primary infection was challenge inoculated with CTV9Δp33-GFP (Fig. 3; a reciprocal experiment in which the GFP-tagged deletion mutant was used for primary inoculation and the RFP-tagged virus was used as the challenge led to results similar to those described be-

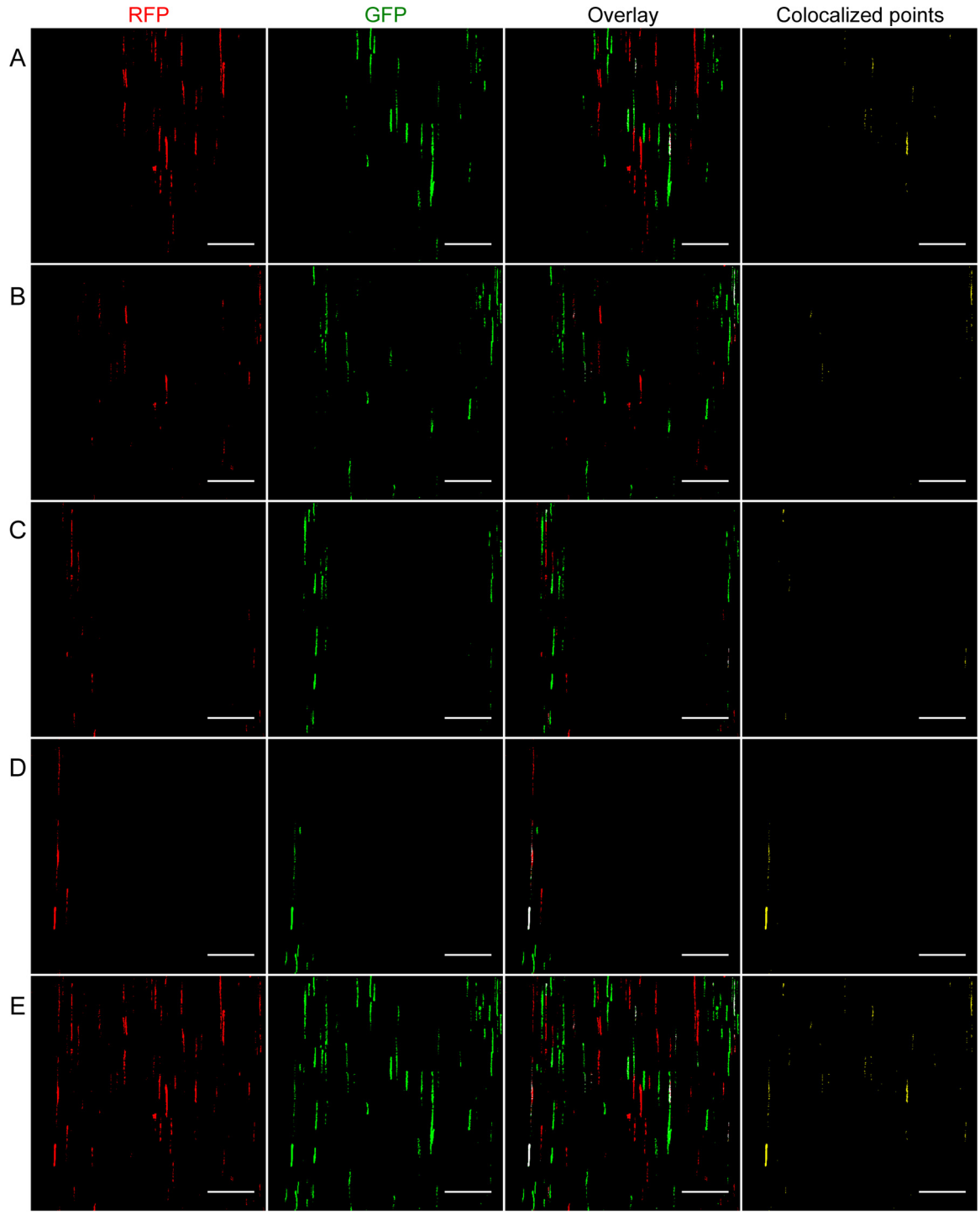

FIG 4 Observation of fluorescence in phloem-associated cells of *C. macrophylla* trees upon sequential inoculation with CTV variants. Trees were first inoculated with CTV9Δp33-RFP and then challenged with CTV9Δp33-GFP. Observations were done at 12 weeks after challenge inoculation on the internal surface of bark of the newly developed flushes using a confocal laser scanning fluorescence microscope. Five sequential optical sections at different depths within the z-stack (sections 8 to 12 [A], 18 to 22 [B], 28 to 32 [C], and 38 to 42 [D]) were merged separately in the green and red channels to count the number of cells infected by each virus. (E) z-projection of 50 sections. Bars = 300 μm.

low). The distribution of the superinfecting GFP-tagged mutant virus and the primary RFP-tagged virus in doubly infected trees was examined by visual observation of GFP and RFP fluorescence in the bark tissue of the newly developed systemic tissue starting at 2 months postchallenge and compared to the distribution of viruses in singly infected plants.

As we expected, superinfection by CTV9Δp33-GFP was not excluded in the plants preinfected with CTV9Δp33-RFP. Both

virus variants expressed abundant levels of fluorescent marker proteins in the infected phloem-associated cells throughout the bark tissue of the inoculated trees, such that the infected cells were readily identifiable under a fluorescence microscope. Remarkably, CTV9Δp33-RFP and CTV9Δp33-GFP appeared not to be spatially separated within the infected tissues: both viruses were detected in all sampled flushes and in all tissue sections from the same flushes (Fig. 3). Moreover, both viruses were often found to be infecting adjacent cells or cells located in close proximity to each other. Nevertheless, the majority of the infected cells contained only one virus variant: either CTV9Δp33-RFP or CTV9Δp33-GFP. Cells coinfected with both viruses were infrequent (Fig. 3 and 4). In this experiment, we examined many tissue samples from different flushes and from several individual infected trees that were taken at different time points during virus infection over a period of from several months up to 1 year after challenge inoculation. The results of the observations from different sets of samples within each treatment were comparable (Table 1 and data not shown). Importantly, there were no significant changes in the distribution pattern of CTV9Δp33-RFP and CTV9Δp33-GFP in superinfected trees along the course of infection: both viruses continuously showed the apparent lack of within-host and within-tissue segregation, while the frequency of cellular coinfection by the two virus variants remained low.

Distribution of CTV9Δp33-GFP and CTV9Δp33-RFP populations in superinfected hosts. As a next step, we conducted a thorough examination of the numbers of cells infected with CTV9Δp33-RFP or CTV9Δp33-GFP and cells coinfected with both viruses. The numbers of cells infected by each virus found in superinfected trees were compared with those found in plants that were inoculated with only one virus variant.

CTV is a phloem-limited virus and usually infects a proportion of phloem-associated cells even in trees of *C. macrophylla*, one of the most susceptible hosts (55). To obtain an estimate of the average number of cells that are susceptible to infection by a CTV variant in that host, we first analyzed the number of cells infected by GFP- or RFP-tagged p33 deletion mutant viruses in plants that were infected by only one virus. (By the number of infected cells, we refer to the number of cells counted in a tissue section.) At 12 weeks after challenge inoculation, multiple samples of bark tissue were collected from several young flushes of individual *C. macrophylla* trees receiving each treatment and observed using confocal microscopy. Special care was taken to prevent counting of each singly or doubly infected cell more than once (see Materials and Methods for details and Fig. 4).

The numbers of cells infected with either virus in plants inoculated with only one virus variant were comparable, on average being about 110 to 116 cells per 0.3 mm^3 of bark tissue (Table 1). The number of infected cells in CTV9Δp33-RFP- or CTV9Δp33-GFP-inoculated plants was similar to that in plants infected with the GFP-tagged wild-type virus, which averaged at 114.7 ± 22.4 (±1 standard error of the mean [SEM]). Interestingly, in samples from plants that were sequentially infected with the two deletion mutants, the total number of infected cells was also comparable, averaging 100.7 ± 6.4 cells per 0.3 mm^3 of tissue (Table 1). This suggests that the average number of cells within the defined host tissue area that are susceptible to infection by CTV is within the range of the numbers observed in this study. Furthermore, in superinfected plants, which contained both RFP- and GFP-tagged viruses, the distribution of the infected cells in most tissue samples

TABLE 1 Number of phloem-associated cells per section infected by CTV p33 deletion mutants[a]

Treatment	Results for cells infected with:	No. of infected cells/section in the following sample[b]:											
		1	2	3	4	5	6	7	8	9	10	Mean	SEM
A	CTV9Δp33-RFP	154	60	98	66	143	71	159	161	87	100	109.9	12.8
B	CTV9Δp33-GFP	99	143	115	114	92	103	115	176	116	86	115.9	8.3
C	CTV9Δp33-GFP only	73 (0.545)	45 (0.344)	79 (0.745)	50 (0.526)	27 (0.250)	39 (0.506)	48 (0.471)	35 (0.340)	36 (0.439)	57 (0.559)	48.9	5.3
	CTV9Δp33-RFP only	55 (0.410)	77 (0.588)	25 (0.236)	38 (0.400)	46 (0.613)	33 (0.429)	49 (0.480)	66 (0.641)	43 (0.524)	39 (0.382)	47.1	4.9
	Both viruses	6 (0.045)	9 (0.069)	2 (0.019)	7 (0.074)	2 (0.027)	5 (0.065)	5 (0.049)	2 (0.019)	3 (0.037)	6 (0.059)	4.7	0.8
	Total	134	131	106	95	75	77	102	103	82	102	100.7	6.4
MOI		1.070	1.063	1.061	1.070	1.062	1.070	1.069	1.060	1.068	1.070		
95% CI MOI		1.034–1.105	1.031–1.103	1.032–1.101	1.034–1.105	1.031–1.102	1.034–1.105	1.033–1.105	1.030–1.096	1.033–1.102	1.034–1.102		

[a] Bark tissue samples from trees inoculated with CTV9Δp33-RFP (treatment A) or CTV9Δp33-GFP (treatment B) or sequentially inoculated with both viruses (treatment C) were examined for RFP and GFP fluorescence at 12 weeks after challenge using a confocal laser scanning microscope.
[b] Values in parentheses are the frequency of infected cells.

TABLE 2 Parameter estimates and model selection for cellular MOI[a]

Analysis	Model	Parameter estimates (95% CI)	NLL	AIC	ΔAIC	AW
A	2		94.728	189.456	140.309	0
	3	$\Psi = 0.030$ (0.020–0.038)	23.574	49.147		0.660
	4	$\omega = 0.459$ (0.370–0.604)	25.482	52.964	3.816	0.098
	5	$\Psi = 0.030$ (0.021–0.038), $\omega = 1$ (*)	23.574	51.147	2.000	0.243
B	2		51.179	102.357	73.422	0
	4	$\omega = 0.451$ (0.332–0.653)	13.468	28.935		1

[a] For model fitting and selection, analysis A included all Poisson-based models and all the data. Analysis B was performed only on replicate flushes in which the distribution of virus variants over infected cells is random, and hence, models incorporating the spatial segregation of genotypes (models 3 and 5) can be excluded *a priori*. For analysis A there was very little support for the null model (model 2), while the level of support for all other models was similar. Note that for the parameter estimates, model 5 collapses to model 3, suggesting that this model can be ignored altogether. For analysis B, there was strong support for model 4, while the estimate of ω was similar to that in analysis A. NLL, negative log likelihood; ΔAIC, difference in the Akaike information criterion (AIC) between the best-fitting model and the model in question; AW, Akaike weight, which is the probability that a model is the best-supported model out of the set of models; Ψ, a parameter that determines how quickly the spatial segregation of virus genotypes occurs over time; ω, a parameter that determines the magnitude of superinfection exclusion (see Materials and Methods); *, the lower and upper values of the 95% CI coincide with the parameter estimate.

was such that, on average, half of the susceptible cells were infected with one virus variant, while the other half contained the second virus (Table 1). The percentage of cells coinfected with both CTV9Δp33-GFP and CTV9Δp33-RFP was low: 4.7% ± 0.8% of all infected cells (Table 1; Fig. 4).

Model selection-based approach to explain the low level of cellular coinfection in a superinfected host. Counts of singly infected and coinfected cells (Table 1) were used to calculate the CTV cellular MOI. To this end, we used the simplest statistical model described previously (52), so-called model 1. An MOI value was calculated for each of the samples for which data are provided in Table 1. MOI values were all very low and ranged from 1.060 to 1.070, with an average value of 1.066 ± 0.001 (±1 SEM). These low MOI values could be caused by SIE at the cellular level, but they could also result from low infection levels in the superinfected host plants or from spatial segregation of the two virus genotypes that lowers the frequency of cellular coinfection as the two virus variants become physically separated in different parts of the plant, due to genetic drift, and, therefore, do not have access to the same cells. To determine which explanation best supports the data, we performed model selection on four Poisson-based models of MOI: the null model (model 2), a model incorporating spatial segregation of virus genotypes over time (model 3), a model incorporating SIE (model 4), and a model combining spatial segregation and SIE (model 5). Other mechanisms affecting MOI (i.e., spatial aggregation of infected cells and differences in host cell vulnerability) were not considered because they lead to high levels of cellular coinfection (52). Whereas Model 2 was poorly supported by the data, support for all other models was similar (Table 2, analysis A). Therefore, MOI model selection in itself could show only that there were significant deviations from the null model, but it could not identify what mechanisms might be responsible for these deviations.

Spatial segregation of the two virus variants would result in patches of cells infected by only one virus variant. However, both virus variants were always observed in all bark tissue samples, suggesting that there was no tissue-level segregation. To test whether there might be spatial segregation at the cellular level, we considered whether the spatial distribution of both virus variants over infected regions appeared to be random, using a resampling approach. If there is spatial segregation, we would expect to see variants distributed nonrandomly over infected regions, which was tested using the average-distance-to-nearest-neighbor ratio (59). In the majority of tissue sections, we observed a random distribution of virus variants over infected regions (Table 3). Only in one case, however, was the distribution of virus variants over infected regions nonrandom for all merged sections tested (sample 8 in Table 3), although three sections showed aggregation and one showed overdispersion. Moreover, the frequency of coinfected cells in samples in which all sections showed a random distribution of the two viruses was not significantly different from that in samples that contained occasional sections with a nonrandom distribution of those virus variants (by the test of equal proportions with 1 degree of freedom, $\chi^2 = 0.004$ and $P = 0.949$). Therefore, a quantitative analysis of the spatial distribution of the virus variants provided results that largely concurred with the initial observations, confirming that for most samples there was no evidence for nonrandom mixing of the genotypes, thus suggesting that spatial segregation of virus variants may not contribute substantially to the observed low levels of cellular coinfection in superinfected plants.

To test this idea, we repeated the model selection procedure using only data from flushes where virus variants appeared to be randomly distributed in all merged sections. Models 3 and 5 could then be excluded *a priori*, given that the virus variants were well mixed. Model 4, incorporating SIE, was much better supported than the null model 2 (Table 2, analysis B). Note that using only partial data for this second analysis is a conservative approach. We excluded those data for which we could not be absolutely sure that the two virus variants were spatially well mixed, to avoid erroneously attributing any deviations from model 2, the null model, to SIE. We can therefore conclude that the data provide support for the occurrence of SIE at the cellular level, given the low estimates of cellular MOI and the fact that competing hypotheses explaining the low levels of cellular coinfection can be discounted.

DISCUSSION

SIE has been studied for a number of different viruses. Most studies with animal and human viruses examined the phenomenon at the cellular level. Therefore, the described mechanisms appeared to be limited to those that modulate exclusion, as the secondary virus aims to infect a cell that has been already occupied. Such mechanisms have been identified at various stages of the viral life cycle, including receptor-mediated attachment, penetration, and subsequent disassembly, translation, and replication steps (1–3, 9, 12, 19, 60). Those, however, would apparently work only in cells

TABLE 3 Resampling analysis of the distribution of virus variants over infected cells[a]

Sample	Sections	*R* value			
		CTV9Δp33-GFP		CTV9Δp33-RFP	
		Observed	CI resampled	Observed	CI resampled
1	8–12	0.609	0.604–0.951[A]	0.768	0.768–0.887[A]
	18–22	0.921	0.674–1.086	0.464	0.464–1.741[B]
	28–32	0.490	0.490–1.654	0.506	0.253–2.856
	38–42	0.310	0.310–0.465	0.376	0.358–0.450
2	8–12	0.899	0.837–1.021	0.982	0.905–1.029
	18–22	0.960	0.795–1.040	0.532*	0.576–1.228[C]
	28–32	1.637	0.501–1.803	0.566	0.537–1.610
	38–42	0.379	0.379–0.423	0.435	0.435–0.435
3	8–12	1.218	0.918–1.258	3.802	0.365–4.050
	18–22	1.112	1.070–1.179	0.851	0.837–1.274
	28–32	0.988	0.951–1.063	0.802	0.777–1.079
	38–42	0.785	0.725–0.955	0.721	0.696–0.963
4	8–12	0.787	0.769–0.825	0.633	0.598–0.864
	18–22	0.795	0.736–0.928	0.731	0.676–0.934
	28–32	0.741	0.719–0.946	0.786	0.734–0.932
	38–42	0.607	0.607–0.719	0.627	0.593–0.719
5	8–12	0.430	0.335–0.608	0.503	0.490–0.550
	18–22	0.283	0.283–2.573	1.949	0.379–1.985
	28–32	0.464	0.397–0.681	1.704*	0.379–1.680[B]
	38–42	0.376*	0.487–1.575[C]	1.150*	0.998–1.102[C]
6	8–12	0.882	0.867–0.947	0.753	0.677–0.900
	18–22	1.284*	0.765–1.040[C]	0.910	0.693–0.983
	28–32	0.867*	0.872–1.088[B]	0.988	0.925–1.073
	38–42	0.866*	0.890–1.072[A]	0.897	0.869–1.051
7	8–12	0.888	0.847–0.935	0.716*	0.721–0.928[C]
	18–22	0.718	0.560–1.197	1.075	0.538–1.212
	28–32	0.580	0.580–0.641	0.405	0.306–2.244
	38–42	0.438	0.438–0.475	0.438	0.219–0.693
8	8–12	0.537*	0.611–0.894	0.969	0.912–0.965
	18–22	0.639*	0.658–1.002[B]	0.969	0.911–0.990
	28–32	0.499*	0.547–1.057[A]	0.878	0.748–0.927
	38–42	1.400*	0.440–1.363[C]	0.909	0.711–0.953
9	8–12	0.799	0.686–0.859	0.773	0.765–0.883
	18–22	0.517	0.438–1.169	1.343	0.335–1.445
	28–32	1.632	0.395–1.898	0.849	0.849–0.891
	38–42	1.700	0.376–1.784	0.633	0.663–0.686
10	8–12	2.377	0.249–2.775	0.438	0.438–0.520
	18–22	0.497	0.374–1.645	0.632	0.632–0.664
	28–32	0.835	0.577–0.845	0.561	0.487–0.979
	38–42	0.580	0.580–0.743[A]	0.704	0.704–0.755

[a] For each merged section, we compared the observed value of the average nearest-neighbor ratio (*R*) to the CI for predicted *R* values obtained by resampling the distribution of virus variants over all infected cells. A Holm-Bonferroni correction to the CI was made. In most cases, the observed *R* values fell inside the corresponding CI, indicating random spatial distribution. For those cases in which the observed *R* value felt outside of the 95% CI (indicated with an asterisk), we sequentially considered the 97.5% CI ([A]), 98.33% CI ([B]), and 98.75% CI ([C]). *R* values were either less than the expected value, suggesting the clustering of virus variants and therefore spatial aggregation (eight cases), or greater than the expected value, suggesting spatial overdispersion of infected cells (four cases).

preinfected with the primary virus, leaving uninfected cells susceptible to the secondary virus. On the other hand, a model that could explain SIE at both the cellular and the systemic levels has been proposed for a number of plant viruses. According to this model, upon infection the primary virus acts as an elicitor of RNA silencing, a host defense mechanism which recognizes and destroys homologous sequences, such as those present in the genomes of closely related viruses invading the same host, thus preventing the secondary infection by other viruses (7, 9, 24, 25). RNA silencing is initially triggered in cells that became infected with the primary virus, where viral double-stranded RNA, such as replicative intermediates or structured regions in the virus genome, is recognized by the host machinery and processed into small interfering RNAs (siRNAs) (61–63). The siRNAs then guide sequence-specific degradation of the viral RNA in these cells. Translocation of siRNAs into the neighboring or more distant noninfected cells leads to protection of noninfected cells and, therefore, generates RNA-based immunity against a closely related virus at the systemic level.

The data presented here provide new insights into the SIE phenomenon. Our results show that the viral p33 protein mediates exclusion at the systemic (whole-organism) level, while exclusion at the cellular level still occurs in its absence. Examination of the distribution of GFP- and RFP-tagged CTV variants, both lacking the p33 protein, upon their sequential inoculation into citrus trees showed that in superinfected plants only a small fraction (~4.7%) of infected cells was coinfected with both virus variants. There are several plausible explanations for the scarcity of doubly infected cells, among which is the action of mechanisms preventing superinfection of already infected cells. Additionally, other mechanisms decreasing the likelihood of two different virus genomes replicating in the same cell may be considered. Those include a low virus titer limiting the MOI, the spatial segregation of virus variants, and exclusion through competition upon simultaneous invasion into a cell. However, the last three models do not seem to be well supported by our observations. As we showed previously, with the wild-type CTV used for primary infection, the exclusion of the secondary infection by the homologous virus was absolute: no trace of the challenge virus was found in preinfected trees (44). Infection by the challenge virus appeared to be excluded both in cells infected with the primary virus and in cells that were not infected. According to the observations obtained from several studies, CTV9Δp33-GFP, CTV9Δp33-RFP, and the wild-type virus exhibit a similar ability to infect, multiply, and spread throughout *C. macrophylla* plants (38, 45; results of this study). All three viruses accumulated at similar titers in the infected trees, and the numbers of cells infected by the deletion mutants and the wild-type virus in singly inoculated plants were comparable. These data suggest that the loss of the ability of the deletion mutants to exclude each other at the whole-plant level cannot be explained simply by a reduction in viral invasiveness, and neither can the low incidence of cellular coinfection in the superinfected plants be attributed to many more susceptible cells remaining unoccupied upon CTV9Δp33 infection, since the number of those should be similar to that upon infection with the wild-type virus. The latter conclusion is also supported by the observation that the number of susceptible cells in the host tissue could be limited: in doubly infected plants, the total number of infected cells was not greater than that in singly infected plants; each of the two deletion mutants infected approximately half the number of cells in com-

parison with the number infected in singly inoculated plants (Table 1), yet the inoculum pressure for viruses upon generating singly and doubly infected plants was comparable.

Similarly, the exclusion through competition at the within-cell level following simultaneous invasion did not appear to play a determining role in the observed rareness of cellular coinfections. Each virus variant was as competitive as the other and wild-type CTV. Moreover, the fluorescence levels in cells infected with either virus were similar. Additionally, when cells were coinfected, we typically observed reasonably high levels of expression of each fluorescent protein, again suggesting that the two variants were not displacing each other at the cellular level. Therefore, it would be likely that upon simultaneous entry into a cell, both variants have a nearly equal probability of establishing an infection that would result in cells replicating distinct virus genomes. This situation appears to have occurred in a low percentage of cells found to be coinfected with the GFP- and RFP-tagged mutants.

Both GFP- and RFP-tagged p33 deletion mutants were always found in the same plant organs (flushes), appeared to be well mixed within the same sections of tissue, and were often seen occupying neighboring cells. Moreover, multiple observations taken as the infection of the host progressed over time showed the apparent lack of the within-host and within-tissue segregation of the two virus variants, allowing us to conclude that spatial separation appeared not to be a factor that determined low levels of cellular coinfection by the GFP- and RFP-tagged p33 deletion mutants. The lack of spatial structuring of viral populations observed in plants superinfected by the two CTV variants is an intriguing observation that raises a special interest *per se*. This situation greatly differs from what was reported for other viruses of both animals and plants. For instance, it was demonstrated that subpopulations of HCV appear to be unevenly distributed in tissues of the same host (64). For a number of plant viruses, analysis of plant host colonization with identical but differentially labeled virus variants showed that they establish infection in separate tissue clusters in the inoculated leaves and the segregation of the virus variants increases as they move systemically (65, 66). Another remarkable example was presented in a study that involved plum pox virus in a *Prunus* tree, in which distinct virus populations were found to be occupying different branches within this perennial host plant (67). In contrast to these reports, we did not find spatial segregation of the two CTV p33 deletion mutants in host tissues in superinfected plants. A possible explanation for this observation is that a lack of SIE at the systemic level in the case of these mutant viruses could be a factor that explains their unstructured distribution within a host. More studies, however, will be required to elucidate the effect of SIE and other driving forces on the structure of virus populations at the intrahost level.

The data presented here suggest that SIE by CTV operates at two levels, the cellular and the whole-organism levels, likely by two distinct mechanisms that could function independently. The viral p33 protein mediates the exclusion at the whole-organism level, while it does not appear to be required for exclusion at the cellular level. Thus, another mechanism must operate at the cellular level. Whether this mechanism shares similar features with one of the mechanisms described for other plant or animal viruses or is unique remains to be determined.

ACKNOWLEDGMENTS

This research was supported by the National Science Foundation under grant number 1050883 (to S. Y. Folimonova). Work in Valencia, Spain, was supported by grant BFU2012-30805 (to S. F. Elena) and by a Juan de la Cierva postdoctoral fellowship (JCI-2011-10379, to M. P. Zwart), both from the Spanish Ministerio de Economía y Competitividad.

Any opinions, findings, and conclusions or recommendations expressed in this material are those of the authors and do not necessarily reflect the views of the National Science Foundation.

REFERENCES

1. **Steck FT, Rubin H.** 1966. The mechanism of interference between an avian leukosis virus and Rous sarcoma virus. I. Establishment of interference. Virology **29:**628–641.
2. **Steck FT, Rubin H.** 1966. The mechanism of interference between an avian leukosis virus and Rous sarcoma virus. II. Early steps of infection by RSV of cells under conditions of interference. Virology **29:**642–653.
3. **Adams RH, Brown DT.** 1985. BHK cells expressing Sindbis virus-induced homologous interference allow the translation of nonstructural genes of superinfecting virus. J. Virol. **54:**351–357.
4. **Strauss JH, Strauss EG.** 1994. The alphaviruses: gene expression, replication, and evolution. Microbiol. Rev. **58:**491–562.
5. **Karpf AR, Lenches E, Strauss EG, Strauss JH, Brown DT.** 1997. Superinfection exclusion of alphaviruses in three mosquito cell lines persistently infected with Sindbis virus. J. Virol. **71:**7119–7123.
6. **Singh IR, Suomalainen M, Varadarajan S, Garoff H, Helenius A.** 1997. Multiple mechanisms for the inhibition of entry and uncoating of superinfecting Semliki Forest virus. Virology **231:**59–71. http://dx.doi.org/10.1006/viro.1997.8492.
7. **Hull R.** 2002. Matthews' plant virology, 4th ed. Academic Press, New York, NY.
8. **Geib T, Sauder C, Venturelli S, Hassler C, Staeheli P, Schewemmle M.** 2003. Selective virus resistance conferred by expression of Borna disease virus nucleocapsid components. J. Virol. **77:**4283–4290. http://dx.doi.org/10.1128/JVI.77.7.4283-4290.2003.
9. **Lee YM, Tscherne DM, Yun SI, Frolov I, Rice CM.** 2005. Dual mechanisms of pestiviral superinfection exclusion at entry and RNA replication. J. Virol. **79:**3231–3242. http://dx.doi.org/10.1128/JVI.79.6.3231-3242.2005.
10. **Gal-On A, Shiboleth YM.** 2006. Cross protection, p 261–288. *In* Loebenstein G, Carr JP (ed), Natural resistance mechanisms of plants to viruses. Springer, Dordrecht, The Netherlands.
11. **Michel N, Allespach I, Venzke S, Fackler OT, Keppler OT.** 2005. The Nef protein of human immunodeficiency virus establishes superinfection immunity by a dual strategy to downregulate cell-surface CCR5 and CD4. Curr. Biol. **15:**714–723. http://dx.doi.org/10.1016/j.cub.2005.02.058.
12. **Tscherne DM, Evans MJ, von Hahn T, Jones CT, Stamataki Z, McKeating JA, Lindenbach BD, Rice CM.** 2007. Superinfection exclusion in cells infected with hepatitis C virus. J. Virol. **81:**3693–3703. http://dx.doi.org/10.1128/JVI.01748-06.
13. **Zou G, Zhang B, Lim PY, Yuan ZM, Bernard KA, Shi PY.** 2009. Exclusion of West Nile virus superinfection through RNA replication. J. Virol. **83:**11765–11776. http://dx.doi.org/10.1128/JVI.01205-09.
14. **Claus C, Tzeng WP, Liebert UG, Frey TK.** 2007. Rubella virus-induced superinfection exclusion studied in cells with persisting replicons. J. Gen. Virol. **88:**2769–2773. http://dx.doi.org/10.1099/vir.0.83092-0.
15. **Nowak MA, May RM.** 1994. Superinfection and the evolution of parasite evolution. Proc. Biol. Sci. **255:**81–89. http://dx.doi.org/10.1098/rspb.1994.0012.
16. **Frank SA.** 2001. Multiplicity of infection and the evolution of hybrid incompatibility in segmented viruses. Heredity **87:**522–529. http://dx.doi.org/10.1046/j.1365-2540.2001.00911.x.
17. **Formella S, Jehle C, Sauder C, Staeheli P, Schewemmle M.** 2000. Sequence variability of Borna disease virus: resistance to superinfection may contribute to high genome stability in persistently infected cells. J. Virol. **74:**7878–7883. http://dx.doi.org/10.1128/JVI.74.17.7878-7883.2000.
18. **Huang IC, Li W, Sui J, Marasco W, Choe H, Farzan M.** 2008. Influenza A virus neuraminidase limits viral superinfection. J. Virol. **82:**4834–4843. http://dx.doi.org/10.1128/JVI.00079-08.
19. **Schaller T, Appel N, Koutsoudakis G, Kallis S, Lohmann V, Piet-**

schmann T, Bartenschlager R. 2007. Analysis of hepatitis C virus superinfection exclusion by using novel fluorochrome gene-tagged viral genomes. J. Virol. **81:**4591–4603. http://dx.doi.org/10.1128/JVI.02144-06.
20. **Nethe M, Berkhout B, van der Kuyl AC.** 2005. Retroviral superinfection resistance. Retrovirology **2:**52. http://dx.doi.org/10.1186/1742-4690-2-52.
21. **Laskus T, Wang LF, Radkowski M, Vargas H, Nowicki M, Wilkinson J, Rakela J.** 2001. Exposure of hepatitis C virus (HCV) RNA-positive recipients to HCV RNA-positive blood donors results in rapid predominance of a single donor strain and exclusion and/or suppression of the recipient strain. J. Virol. **75:**2059–2066. http://dx.doi.org/10.1128/JVI.75.5.2059-2066.2001.
22. **Walters KA, Joyce MA, Addison WR, Fischer KP, Tyrrell DLJ.** 2004. Superinfection exclusion in duck hepatitis B virus infection is mediated by the large surface antigen. J. Virol. **78:**7925–7937. http://dx.doi.org/10.1128/JVI.78.15.7925-7937.2004.
23. **Ramírez S, Pérez-del-Pulgar S, Carrión JA, Coto-Llerena M, Mensa L, Dragun J, García-Valdecasas JC, Navasa M, Forns X.** 2010. Hepatitis C virus superinfection of liver grafts: a detailed analysis of early exclusion of non-dominant virus strains. J. Gen. Virol. **91:**1183–1188. http://dx.doi.org/10.1099/vir.0.018929-0.
24. **Ratcliff F, Harrison BD, Baulcombe DC.** 1997. A similarity between viral defense and gene silencing in plants. Science **276:**1558–1560. http://dx.doi.org/10.1126/science.276.5318.1558.
25. **Ratcliff F, MacFarlane SA, Baulcombe DC.** 1999. Gene silencing without DNA: RNA-mediated cross-protection between viruses. Plant Cell **11:**1207–1215.
26. **Ding SW, Voinnet O.** 2007. Antiviral immunity directed by small RNAs. Cell **30:**413–426. http://dx.doi.org/10.1016/j.cell.2007.07.039.
27. **Voinnet O.** 2005. Induction and suppression of RNA silencing: insights from viral infections. Nat. Rev. Genet. **6:**206–220. http://dx.doi.org/10.1038/nrg1555.
28. **Bar-Joseph M, Garnsey SM, Gonsalves D.** 1979. The closteroviruses: a distinct group of elongated plant viruses. Adv. Virus Res. **25:**93–168. http://dx.doi.org/10.1016/S0065-3527(08)60569-2.
29. **Dolja VV, Karasev AV, Koonin EV.** 1994. Molecular biology and evolution of closteroviruses: sophisticated build-up of large RNA genomes. Annu. Rev. Phytopathol. **32:**261–285. http://dx.doi.org/10.1146/annurev.py.32.090194.001401.
30. **Agranovsky AA.** 1996. Principles of molecular organization, expression, and evolution of closteroviruses: over the barriers. Adv. Virus Res. **47:**119–158. http://dx.doi.org/10.1016/S0065-3527(08)60735-6.
31. **Karasev AV.** 2000. Genetic diversity and evolution of closteroviruses. Annu. Rev. Phytopathol. **38:**293–324. http://dx.doi.org/10.1146/annurev.phyto.38.1.293.
32. **Dolja VV, Kreuze JF, Valkonen JPT.** 2006. Comparative and functional genomics of closteroviruses. Virus Res. **117:**38–51. http://dx.doi.org/10.1016/j.virusres.2006.02.002.
33. **Pappu HR, Karasev AV, Anderson EJ, Pappu SS, Hilf ME, Febres VJ, Eckloff RMG, McCaffery M, Boyko V, Gowda S, Dolja VV, Koonin EV, Gumpf DJ, Cline KC, Garnsey SM, Dawson WO, Lee RF, Niblett CL.** 1994. Nucleotide sequence and organization of eight open reading frames of the citrus tristeza closterovirus genome. Virology **199:**35–46. http://dx.doi.org/10.1006/viro.1994.1095.
34. **Karasev AV, Boyko VP, Gowda S, Nikolaeva OV, Hilf ME, Koonin EV, Niblett CL, Cline K, Gumpf DJ, Lee RF, Garnsey SM, Lewandowski DJ, Dawson WO.** 1995. Complete sequence of the *Citrus tristeza virus* RNA genome. Virology **208:**511–520. http://dx.doi.org/10.1006/viro.1995.1182.
35. **Hilf ME, Karasev AV, Pappu HR, Gumpf DJ, Niblett CL, Garnsey SM.** 1995. Characterization of *Citrus tristeza virus* subgenomic RNAs in infected tissue. Virology **208:**576–582. http://dx.doi.org/10.1006/viro.1995.1188.
36. **Karasev AV, Hilf ME, Garnsey SM, Dawson WO.** 1997. Transcriptional strategy of closteroviruses: mapping the 5′ termini of the *Citrus tristeza virus* subgenomic RNAs. J. Virol. **71:**6233–6236.
37. **Satyanarayana T, Gowda S, Ayllón MA, Dawson WO.** 2003. Frameshift mutations in infectious cDNA clones of *Citrus tristeza virus*: a strategy to minimize the toxicity of viral sequences to *Escherichia coli*. Virology **313:**481–491. http://dx.doi.org/10.1016/S0042-6822(03)00387-8.
38. **Tatineni S, Robertson CJ, Garnsey SM, Bar-Joseph M, Gowda S, Dawson WO.** 2008. Three genes of *Citrus tristeza virus* are dispensable for infection and movement throughout some varieties of citrus trees. Virology **376:**297–307. http://dx.doi.org/10.1016/j.virol.2007.12.038.
39. **Lu R, Folimonov A, Shintaku M, Li WX, Falk BW, Dawson WO, Ding SW.** 2004. Three distinct suppressors of RNA silencing encoded by a 20-kb viral RNA genome. Proc. Natl. Acad. Sci. U. S. A. **101:**15742–15747. http://dx.doi.org/10.1073/pnas.0404940101.
40. **Tatineni S, Robertson CJ, Garnsey SM, Dawson WO.** 2011. A plant virus evolved by acquiring multiple nonconserved genes to extend its host range. Proc. Natl. Acad. Sci. U. S. A. **108:**17366–17371. http://dx.doi.org/10.1073/pnas.1113227108.
41. **Harper SJ.** 2013. *Citrus tristeza virus*: evolution of complex and varied genotypic groups. Front. Microbiol. **4:**93. http://dx.doi.org/10.3389/fmicb.2013.00093.
42. **Folimonov AS, Folimonova SY, Bar-Joseph M, Dawson WO.** 2007. A stable RNA virus-based vector for citrus trees. Virology **368:**205–216. http://dx.doi.org/10.1016/j.virol.2007.06.038.
43. **Dawson WO, Folimonova SY.** 2013. Virus-based transient expression vectors for woody crops: a new frontier for vector design and use. Annu. Rev. Phytopathol. **51:**321–337. http://dx.doi.org/10.1146/annurev-phyto-082712-102329.
44. **Folimonova SY, Robertson CJ, Shilts T, Folimonov AS, Hilf ME, Garnsey SM, Dawson WO.** 2010. Infection with strains of *Citrus tristeza virus* does not exclude superinfection by other strains of the virus. J. Virol. **84:**1314–1325. http://dx.doi.org/10.1128/JVI.02075-09.
45. **Folimonova SY.** 2012. Superinfection exclusion is an active virus-controlled function that requires a specific protein. J. Virol. **86:**5554–5561. http://dx.doi.org/10.1128/JVI.00310-12.
46. **Gowda S, Satyanarayana T, Robertson CJ, Garnsey SM, Dawson WO.** 2005. Infection of citrus plants with virions generated in *Nicotiana benthamiana* plants agroinfiltrated with a binary vector based *Citrus tristeza virus*, p 23–33. *In* Hilf ME, Duran-Vila N, Rocha-Peña MA (ed), Proceedings of the 16th Conference of the International Organization of Citrus Virologists. International Organization of Citrus Virologists, Riverside, CA.
47. **Martin K, Kopperud K, Chakrabarty R, Banerjee R, Brooks R, Goodin MM.** 2009. Transient expression in *Nicotiana benthamiana* fluorescent marker lines provides enhanced definition of protein localization, movement and interactions in planta. Plant J. **59:**150–162. http://dx.doi.org/10.1111/j.1365-313X.2009.03850.x.
48. **Cañizares MC, Navas-Castillo J, Moriones E.** 2008. Multiple suppressors of RNA silencing encoded by both genomic RNAs of the crinivirus, Tomato chlorosis virus. Virology **379:**168–174. http://dx.doi.org/10.1016/j.virol.2008.06.020.
49. **Ambrós S, El-Mohtar C, Ruiz-Ruiz S, Peña L, Guerri J, Dawson WO, Moreno P.** 2011. Agroinoculation of *Citrus tristeza virus* causes systemic infection and symptoms in the presumed nonhost *Nicotiana benthamiana*. Mol. Plant Microbe Interact. **24:**1119–1131. http://dx.doi.org/10.1094/MPMI-05-11-0110.
50. **Robertson CJ, Garnsey SM, Satyanarayana T, Folimonova S, Dawson WO.** 2005. Efficient infection of citrus plants with different cloned constructs of *Citrus tristeza virus* amplified in *Nicotiana benthamiana* protoplasts, p 187–195. *In* Hilf ME, Duran-Vila N, Rocha-Peña MA (ed), Proceedings of the 16th Conference of the International Organization of Citrus Virologists. International Organization of Citrus Virologists, Riverside, CA.
51. **Garnsey SM, Cambra M.** 1991. Enzyme-linked immunosorbent assay (ELISA) for citrus pathogens, p 193–216. *In* Roistacher CN (ed), Graft-transmissible diseases of citrus. Handbook for detection and diagnosis. FAO, Rome, Italy.
52. **Zwart MP, Tromas N, Elena SF.** 2013. Model-selection-based approach for calculating cellular multiplicity of infection during virus colonization of multi-cellular hosts. PLoS One **8:**e64657. http://dx.doi.org/10.1371/journal.pone.0064657.
53. **González-Jara P, Fraile A, Canto T, García-Arenal F.** 2009. The multiplicity of infection of a plant virus varies during colonization of its eukaryotic host. J. Virol. **83:**7487–7494. http://dx.doi.org/10.1128/JVI.00636-09.
54. **Sokal RR, Rohlf FJ.** 1995. Biometry, 3rd ed, p 686–697. WH Freeman & Co, New York, NY.
55. **Folimonova SY, Folimonov AS, Tatineni S, Dawson WO.** 2008. *Citrus tristeza virus*: survival at the edge of the movement continuum. J. Virol. **82:**6546–6556. http://dx.doi.org/10.1128/JVI.00515-08.
56. **Schneider CA, Rasband WS, Eliceiri KW.** 2012. NIH Image to ImageJ: 25

years of image analysis. Nat. Methods **9:**671–675. http://dx.doi.org/10.1038/nmeth.2089.
57. **Development Core Team R.** 2013. R: a language and environment for statistical computing. R Foundation for Statistical Computing, Vienna, Austria.
58. **Baddeley A, Turner R.** 2013. Spatstat: spatial point pattern analysis, model-fitting, simulation, tests. R Foundation for Statistical Computing, Vienna, Austria.
59. **Clark PJ, Evans C.** 1954. Distance to nearest neighbor as a measure of spatial relationships in populations. Ecology **35:**445–453. http://dx.doi.org/10.2307/1931034.
60. **Webster B, Ott M, Green WC.** 2013. Evasion of superinfection exclusion and elimination of primary viral RNA by an adapted strain of hepatitis C virus. J. Virol. **87:**13354–13369. http://dx.doi.org/10.1128/JVI.02465-13.
61. **Voinnet O.** 2001. RNA silencing as a plant immune system against viruses. Trends Genet. **17:**449–459. http://dx.doi.org/10.1016/S0168-9525(01)02367-8.
62. **Baulcombe D.** 2004. RNA silencing in plants. Nature **431:**356–363. http://dx.doi.org/10.1038/nature02874.
63. **Ding SW.** 2010. RNA-based antiviral immunity. Nat. Rev. Immunol. **10:**623–644. http://dx.doi.org/10.1038/nri2824.
64. **Laskus T, Radkowski M, Wang LF, Nowicki M, Rakela J.** 2000. Uneven distribution of hepatitis C virus quasispecies in tissues from subjects with end-stage liver disease: confounding effect of viral adsorption and mounting evidence for the presence of low-level extrahepatic replication. J. Virol. **74:**1014–1017. http://dx.doi.org/10.1128/JVI.74.2.1014-1017.2000.
65. **Dietrich C, Maiss E.** 2003. Fluorescent labelling reveals spatial separation of potyvirus populations in mixed infected *Nicotiana benthamiana* plants. J. Gen. Virol. **84:**2871–2876. http://dx.doi.org/10.1099/vir.0.19245-0.
66. **Takahashi T, Sugawara T, Yamatsuta T, Isogai M, Natsuaki T, Yoshikawa N.** 2007. Analysis of the spatial distribution of identical and two distinct virus populations differently labeled with cyan and yellow fluorescent proteins in coinfected plants. Phytopathology **97:**1200–1206. http://dx.doi.org/10.1094/PHYTO-97-10-1200.
67. **Jridi C, Martin JF, Marie-Jeanne V, Labonne G, Blanc S.** 2006. Distinct viral populations differentiate and evolve independently in a single perennial host plant. J. Virol. **80:**2349–2357. http://dx.doi.org/10.1128/JVI.80.5.2349-2357.2006.